

Model Mixing Using Bayesian Additive Regression Trees

John C. Yannotty, Thomas J. Santner, Richard J. Furnstahl, and Matthew T. Pratola

The Ohio State University

January 9, 2023

Abstract

In modern computer experiment applications, one often encounters the situation where various models of a physical system are considered, each implemented as a simulator on a computer. An important question in such a setting is determining the best simulator, or the best combination of simulators, to use for prediction and inference. Bayesian model averaging (BMA) and stacking are two statistical approaches used to account for model uncertainty by aggregating a set of predictions through a simple linear combination or weighted average. Bayesian model mixing (BMM) extends these ideas to capture the localized behavior of each simulator by defining input-dependent weights. One possibility is to define the relationship between inputs and the weight functions using a flexible non-parametric model that learns the local strengths and weaknesses of each simulator. This paper proposes a BMM model based on Bayesian Additive Regression Trees (BART). The proposed methodology is applied to combine predictions from Effective Field Theories (EFTs) associated with a motivating nuclear physics application.

Keywords: Computer Experiments; Effective Field Theories; Model stacking; Uncertainty quantification

1 Introduction

In statistical learning problems, one often considers a set of plausible models, each designed to explain the system of interest. A common practice is to select a best performing model based on some pre-specified criteria. The ensuing inference for quantities of interest is then carried out using the selected model as if it were the true data generating mechanism. The resulting uncertainty

quantification ignores any variability due to the underlying model structure (Draper, 1995). The misrepresentation of uncertainties associated with such quantities can ultimately lead to misguided interpretation or inappropriate decisions. Another shortcoming of the typical approach to modeling is that the resulting inference may strongly depend on the selection criteria. In other words, different sets of criteria could lead to noticeably different final models and inferential results. To account for such uncertainties, one may elect to combine information across the set of models in some manner.

Any model set can be classified into one of three categories: \mathcal{M} -closed, \mathcal{M} -complete, and \mathcal{M} -open (Bernardo and Smith, 2009). The \mathcal{M} -closed setting assumes the true model, \mathcal{M}_\dagger , can formally be defined and is contained within the set of models under consideration. In this setting, model selection is appropriate because \mathcal{M}_\dagger can be recovered from the set of models under consideration. The \mathcal{M} -complete setting describes the case where \mathcal{M}_\dagger can formally be defined, however it is not contained in the model set. Similarly, the \mathcal{M} -open case assumes the true model exists and is excluded from the model set. However, in this situation \mathcal{M}_\dagger is further assumed to be intractable and thus cannot be formally defined. Model selection is inappropriate in the latter two cases because one will inevitably select the wrong model to perform inference while simultaneously ignoring the uncertainty induced by this error (Bernardo and Smith, 2009). This work is motivated by applications in nuclear physics which tend to fall within the \mathcal{M} -open class.

Assume a set of K models are considered when studying a particular system of interest. One approach to account for model uncertainty is to combine the information across these K models. This may involve combining the individual point predictions or probability density functions from each model, usually in some additive manner. Traditional approaches utilize global weighting schemes, where each model is weighted by a value intended to reflect overall (global) model performance. In the Bayesian paradigm, the classical global weighting scheme is Bayesian model averaging (BMA) (Raftery et al., 1997), which combines the individual posterior densities from each model using a convex combination. The BMA weights are given by the individual posterior model probabilities, each which can be interpreted as the probability the individual model is the true data generating one. Hence, BMA implicitly assumes the true model is contained within the model set, which renders this method inappropriate outside of the \mathcal{M} -closed setting (Draper, 1995). More recent Bayesian global weighting schemes adopt a model stacking approach, where model weights are assigned to minimize a specified posterior expected loss. This decision theory viewpoint of global weighting can be used for combining point predictions (Le and Clarke, 2017) or probability densities (Yao et al., 2018). Regardless of the implementation, Bayesian stacking methods are

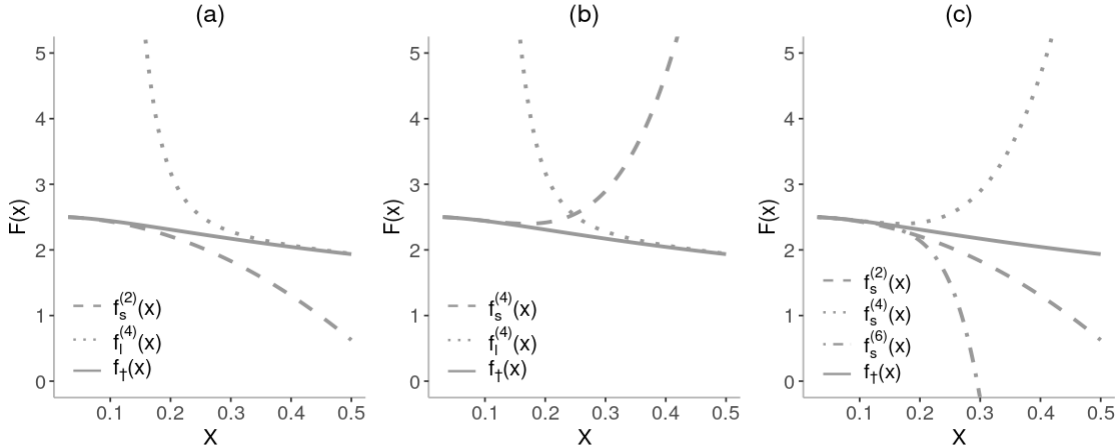


Figure 1: Three different EFT experimental settings. Each panel displays the true physical system (solid) and the EFTs under consideration (non-solid).

appropriate for both the \mathcal{M} -open and \mathcal{M} -closed settings because the weights are chosen based on some pre-specified criteria and do not share the probabilistic interpretation of BMA.

Though global weighting methods are effective, they still might lead to poor approximations of the true system when the individual model performance is localized. In such a case, one may wish to select a weighting scheme that reflects the localized characteristics of the models by constructing input-dependent weights. With input-dependent weights, one would expect an individual model to receive a higher weight in input regions where it exhibits strong predictive performance, while receiving a weight close to zero in regions of poor performance. Localized weighting schemes are more appropriate for the \mathcal{M} -open or \mathcal{M} -complete settings where the true model is better characterized as a localized mixture of the model set under consideration.

This work is motivated by problems in nuclear physics modeled using a technique known as Effective Field Theory (EFT) (Burgess, 2020; Petrov and Blechman, 2016; Georgi, 1993). EFTs are designed to perform well in a particular subregion(s) of the input domain, yet diverge in the rest of the input domain. Prototypes of such models are the weak and strong coupling finite-order expansions for the partition function of the zero-dimensional ϕ^4 theory presented by Honda (2014). Examples of this problem are shown in Figure 1 where the various dashed and dotted lines represent the mean predictions from a finite-order expansion and the solid line denotes the true physical system. One can see that these models are highly accurate descriptions of the true system in some regions of the domain, yet they are unable to provide a globally accurate model. Most EFT problems are examples of the \mathcal{M} -open setting, in that the true underlying description of the

system across the entire domain of interest is intractable and thus it is not contained within the model set. Therefore, multiple EFTs are constructed to recover the true system across subsets of the domain.

To demonstrate why problems falling in the \mathcal{M} -open class may not be suited for model averaging schemes, consider applying BMA to the model set involving the two expansions as shown in Figure 1(a). The resulting posterior mean prediction from BMA still results in a poor estimate of the true system as shown in Figure 2. Essentially, BMA selects the dashed model rather than leveraging the localized strengths contained in the model set.

Given the characteristics of EFTs and the \mathcal{M} -open setting associated with these problems, a simple weighted average of the predictions from each model is insufficient for recovering the true physical system. A better approach is to use an input-dependent weighting scheme which leverages the localized behaviors of each model to ascertain appropriate mean prediction and uncertainty quantification. Such an approach falls under the general class of problems known as Bayesian model mixing (BMM) (Yao et al., 2021).

A key challenge in BMM is to define the relationship between the inputs and the model weight functions. This work proposes a Bayesian treed model which specifies the weight functions as a sum-of-trees. This representation relies on a tree basis of weak learners which are used to capture the localized model behavior. Additionally, this flexible and non-parametric approach allows the user to avoid having to specify a more restrictive model for the weight functions, such as a generalized linear model. Maintaining the traditional conjugacy properties associated with Bayesian Additive Regression Tree (BART) models, the weight functions are regularized via a multivariate Gaussian prior. The prior is calibrated so that the weight functions prefer the interval $[0, 1]$ without imposing any further constraints. Additionally, this framework includes a simple strategy for incorporating prior information about localized model performance when available. All together, this approach highlights the localized behaviors of the candidate models and yields significant improvements in prediction, interpretation, and uncertainty

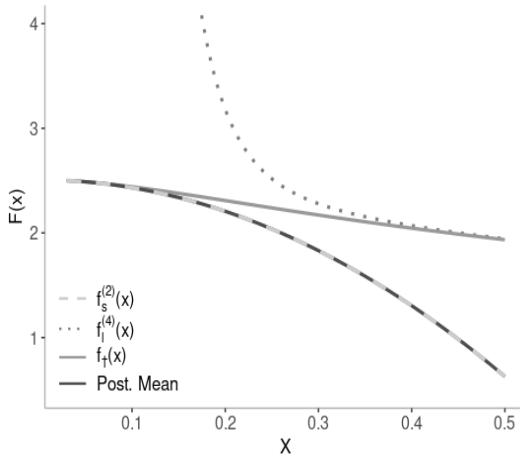


Figure 2: The posterior mean prediction of $f_{\dagger}(x)$ when applying BMA to the 2nd order weak and 4th order strong coupling expansions.

quantification compared to traditional model averaging methods.

The remainder of the paper is organized in the following manner. Section 2 highlights some relevant work related to model averaging and model mixing. Section 3 describes the essential properties of EFTs, while Section 4 outlines the specifics of the proposed BART-based framework. Three motivating EFT examples are presented in Section 5. Finally, Section 6 provides a detailed discussion of the results presented throughout this work.

2 Background

Methods to address model uncertainty have been widely studied throughout the past few decades. The majority of work in this area strives to combine competing models through either mean or density estimation. In either case, the combined result is generally found by taking a linear combination of the individual predictive means or densities from the models under consideration. The weights in this linear combination may or may not depend on the inputs for each model and are learned using the set of training data $\mathcal{D} = \{(x_1, y_1), \dots, (x_n, y_n)\}$. This section briefly reviews some of the popular model averaging and model mixing techniques currently available in the literature.

Bayesian Model Averaging

A classical approach for combining models $\mathcal{M}_1, \dots, \mathcal{M}_K$ is *Bayesian Model Averaging* (Raftery et al., 1997). Suppose Q is a quantity of interest. The posterior density of Q is defined using a convex combination of the posterior densities under each model, $\pi(Q | \mathcal{D}) = \sum_{l=1}^K w_l \pi(Q | \mathcal{D}, \mathcal{M}_l)$. Each weight is defined in terms of its corresponding model evidence, i.e. $w_l = \pi(\mathcal{M}_l | \mathcal{D})$ where

$$\pi(\mathcal{M}_l | \mathcal{D}) = \frac{p(\mathcal{D} | \mathcal{M}_l)\pi(\mathcal{M}_l)}{\sum_{k=1}^K p(\mathcal{D} | \mathcal{M}_k)\pi(\mathcal{M}_k)}$$

and $p(\mathcal{D} | \mathcal{M}_l)$ is the marginal likelihood of the data with respect to the l th model. Though BMA is useful, it has been criticized for emphasizing a fit to the training data as opposed to out-of-sample prediction, asymptotically selecting a single model (inappropriate in the \mathcal{M} -complete and \mathcal{M} -open settings, e.g. Figure 2), and for tending to be sensitive to the prior model probabilities.

Bayesian Mean Stacking

One popular approach for mean estimation is *Stacking*. Some of the earlier works in stacking focused on frequentist approaches for combining point predictions (Breiman, 1996). More recent work has extended stacking to the Bayesian paradigm (Clyde and Iversen, 2013; Le and Clarke, 2017). Given K competing models, the stacked mean for a future observation \tilde{y} at input \tilde{x} is

constructed as a linear combination of individual model predictors

$$E[\tilde{y} | \tilde{x}, \mathcal{D}] = \sum_{l=1}^K w_l f_l(\tilde{x}),$$

where $E[\tilde{y} | \tilde{x}, \mathcal{D}, \mathcal{M}_l] = f_l(\tilde{x})$. When the individual models are unknown, stacking is conducted in a two-step procedure: (i) independently fitting the individual models \mathcal{M}_l , $l = 1, \dots, K$, given the set of training data \mathcal{D} , and (ii) estimating the weights $\mathbf{w} = (w_1, \dots, w_K)^\top$ for the stacked predictor given the fitted models.

In the first step, each model is fit and their corresponding mean predictions, $\hat{f}_l(x_i)$, are obtained at each of the training points. In practice, cross validation techniques are used in this stage to reduce the risk of overfitting the stacked predictor to the data since each model is trained using the identical dataset \mathcal{D} . In the second step, the coefficients $\mathbf{w} = (w_1, \dots, w_K)^\top$ are found via optimization. In the Bayesian paradigm, the weights are selected to minimize the posterior risk for some pre-specified loss function. For example, the squared error loss between the observed data and the stacked predictor at new point \tilde{x} is given by $\hat{\mathbf{w}} = \operatorname{argmin}_{\mathbf{w}} \int \left(\tilde{y} - \sum_{l=1}^K w_l \hat{f}_l(\tilde{x}) \right)^2 p(\tilde{y} | \tilde{x}, \mathcal{D}) d\tilde{y}$. Using the observed data, the posterior risk can be approximated with leave-one-out (LOO) cross validation techniques which allows the stacking weights to be selected by $\hat{\mathbf{w}} = \operatorname{argmin}_{\mathbf{w}} \sum_{i=1}^n \left(y_i - \sum_{l=1}^K w_l \hat{f}_l^{(-i)}(x_i) \right)^2$, where $\hat{f}_l^{(-i)}(x_i)$ is the LOO cross-validation prediction for the i th observation using the l th model as discussed in Le and Clarke (2017).

Additionally, one may choose to modify this loss function to impose a set of conditions on the weights. For example, one may impose a simplex, non-negativity, or sum-to-m constraint on the weights (Le and Clarke, 2017). Other approaches include regularization via a penalty term or a prior (Breiman, 1996; Yang and Dunson, 2014). Such approaches can be useful when the individual model predictions are highly correlated.

Bayesian Complete Stacking

Complete Stacking was introduced in 2018 by Yao et al. (2018) and motivated by the shortcomings of BMA (Yao et al., 2018). Their proposed Bayesian stacking model emphasizes prediction, as the weights are selected to minimize the Kullback-Leibler (KL) divergence between the true predictive density and the stacked predictive density

$$p(\tilde{y} | \tilde{x}) = \sum_{l=1}^K w_l p(\tilde{y} | \tilde{x}, \mathcal{D}, \mathcal{M}_l),$$

where \tilde{y} is a future observation with input \tilde{x} . Similar to mean stacking, the leave-one-out (LOO) cross validated predictive density can be used in place of $p(\tilde{y} | \tilde{x}, \mathcal{D}, \mathcal{M}_l)$ when the individual models

are unknown. Given training data, the weights are constrained to a K -dimensional simplex S_K and estimated as $\hat{\mathbf{w}} = \operatorname{argmax}_{\mathbf{w} \in S_K} \sum_{i=1}^n \log \sum_{l=1}^K w_l p(y_i | x_i, \mathcal{D}^{(-i)}, \mathcal{M}_l)$, where $\mathcal{D}^{(-i)}$ denotes the training set excluding the pair (x_i, y_i) .

Bayesian Hierarchical Stacking

Hierarchical Stacking is a model mixing approach which extends Complete Stacking by defining input-dependent weights that are estimated in a fully Bayesian manner. One way to define the relationship between the inputs and the weight functions is through a parametric model. In this case, one models $K - 1$ unconstrained weight functions,

$$w_l^*(x_i) = \mu_l + \sum_{j=1}^J \alpha_{lj} g_j(x_i),$$

which depend on the sets of hyperparameters $\{\alpha_{lj}\}$ and $\{\mu_l\}$ along with user-specified basis functions $g_j(x_i)$, where $j = 1, \dots, J$ and $l = 1, \dots, K - 1$. The K^{th} function $w_K^*(x_i)$ is set to 0 to serve as a baseline. Then, a softmax transformation is applied to the unconstrained weights in order to confine each model weight to the K -dimensional simplex, namely

$$w_l(x) = \frac{\exp(w_l^*(x))}{\exp(w_1^*(x)) + \dots + \exp(w_K^*(x))} \quad \text{for } l = 1, \dots, K.$$

The methods discussed above outline a number of strategies one can take to combine the information across multiple models. In the setting of EFT experiments, the localized nature of the predictions suggests an input-dependent weighing scheme like Bayesian Hierarchical Stacking is more suitable. However, specifying the required basis functions may not be trivial. Thus, the proposed method will adopt the notion of mean stacking within an additive tree basis model to achieve localized weighting in a flexible and non-parametric manner. But first, the motivating EFT experimental setting is reviewed in more detail.

3 Towards Model Mixing with EFTs

Computer models such as EFTs are typically implemented as simulators which are motivated by the known physics. The theoretical predictions of the physical system are approximations from each simulator plus a discrepancy term, which is designed to account for the remaining unexplained portions of a system. These two components may have specific properties which can be leveraged when working with observational data. This section summarizes these details in the context of EFTs, while a further discussion is provided in the supplementary material.

3.1 Motivating EFT Example

Consider the EFT example where the true physical system is the partition function of the zero-dimensional ϕ^4 theory defined by

$$f_{\dagger}(x) = \int_{-\infty}^{\infty} \exp\left(-\frac{u^2}{2} - x^2 u^4\right) du, \quad (1)$$

where x denotes the coupling constant (Honda, 2014). Two types of finite-order expansions exist for this partition function and are given by (2) and (3) for n_s or $n_l \geq 1$.

$$h_s^{(n_s)}(x) = \sum_{t=0}^{n_s} s_t x^t \quad \text{where } s_t = \begin{cases} \frac{\sqrt{2}\Gamma(t+0.5)}{(t/2)!} (-4)^{(t/2)} & t \text{ is even} \\ 0 & t \text{ is odd} \end{cases} \quad (2)$$

$$h_l^{(n_l)}(x) = \sum_{t=0}^{n_l} l_t x^{-t} \quad \text{where } l_t = \frac{\Gamma(0.5t + 0.25)}{2t!} \left(-\frac{1}{2}\right)^t, \quad t = 0, \dots, n_l. \quad (3)$$

The weak coupling expansion in (2) is an asymptotic Taylor-like series of order n_s centered about zero. Thus, $h_s^{(n_s)}(x)$ will yield high fidelity predictions for smaller coupling constants and diverge as the value increases. The reverse behavior is observed for the strong coupling expansion in (3), $h_l^{(n_l)}(x)$, which is convergent. Example predictions of the physical system using these finite-order expansions can be seen in Figure 1 and are discussed in detail in Section 3.2.

The theoretical predictions of the physical system using the weak and strong coupling expansions are expressed using (4) and (5), respectively.

$$f_s^{(n_s)}(x) = h_s^{(n_s)}(x) + \delta_s^{(n_s)}(x) \quad (4)$$

$$f_l^{(n_l)}(x) = h_l^{(n_l)}(x) + \delta_l^{(n_l)}(x). \quad (5)$$

where the truncation errors $\delta_s^{(n_s)}(x)$ and $\delta_l^{(n_l)}(x)$ are modeled with Gaussian processes (GPs) (Gramacy, 2020; Santner et al., 2018). As described by Melendez et al. (2019), the parameters in both truncation error models are dependent upon the evaluations of their corresponding finite-order expansions (described in (2) and (3), respectively) over a sparse grid of points. The discrepancy model also depends on physical quantities, $Q(x)$ and $y_{\text{ref}}(x)$, which are chosen based on domain expertise. The relationship between these quantities and the discrepancy are summarized in the supplementary material. When $Q(x)$ and $y_{\text{ref}}(x)$ are unknown, one can alternatively use the error approximation described by Sempowski et al. (2022).

The features present in this example from Honda (2014) are commonly found across the landscape of EFT problems. For instance, the physical system can be expressed as an additive model

involving a finite-order expansion and the induced truncation error. The finite-order expansions are designed to provide high fidelity predictions in specific subregions of the domain. There exists a subregion of the domain where none of the finite-order expansions yield accurate theoretical predictions. All together, this motivating example serves as a prototype for the EFTs that may be encountered in a general experimental setting.

3.2 The Model Set for EFT Experiments

One may encounter various experimental settings when working with EFTs. Such scenarios are introduced in the context of the motivating example presented in Section 3.1. First, consider the most basic case where the model set contains a single EFT. With one EFT, the overall predictive accuracy of the true system is poor, despite the good performance in a localized region. For example, suppose the model set \mathcal{M} contains the 2nd order weak coupling expansion $f_s^{(2)}(x)$. Mean predictions constructed from (2) and (4) are shown by the dashed line in Figure 1(a). Clearly, this model is limited to strong predictive accuracy in only the left subregion of the domain.

When available, one can consider different finite-order approximations of the same EFT. For example, consider the 2nd, 4th, and the 6th order coupling expansions which are shown in Figure 1(c). The three models are very similar for lower coupling constants yet drastically differ in the remainder of the domain. Despite each expansion's poor theoretical predictions, one can still leverage the available information to improve the overall prediction of the physical system. For instance, the 2nd and 6th order expansions (dashed and dashed-dotted) are concave functions while the 4th order expansion (dotted) is convex. This suggests the true physical system lies between the expansions under consideration and can be recovered by re-weighting the corresponding predictions.

A third situation is to consider multiple EFTs. In this example, one can consider various finite-order strong coupling expansions in addition to the weak coupling expansions. For example, a model set can contain a finite-order weak coupling expansion (dashed) and the 4th order strong coupling expansion (dotted) as shown in Figures 1(a) and 1(b). The addition of the strong coupling expansion allows for a high fidelity prediction of the physical system to be considered in the rightmost subregion of the domain. The model set listed in panel (a) implies the true system lies between the two expansions. This is particularly useful in the intermediate range where neither of the EFTs are accurate. Meanwhile, the set in panel (b) presents an interesting case where the physical system lies below both EFTs in the intermediate range. In this case, the information in the observational data can be leveraged to help recover the true system.

In this example, the predictions from the weak coupling expansion degrade slowly compared to those from the strong coupling expansions. Consequently, the weak coupling expansions generally appear to have a better overall predictive performance across the entirety of the domain. When combining these two types of EFTs using global weighting schemes such as BMA, the resulting prediction will favor the weak coupling expansion due to its drastic advantage in the overall model performance. The undesirability of the BMA solution is evident in Figure 2, which demonstrates that BMA effectively matches the 2nd order weak coupling expansion. Hence, a weighting scheme which captures the localized behaviors of each model is preferred in the EFT setting.

The proceeding sections consider a general set of K different EFTs, which are denoted by $f_1(x), \dots, f_K(x)$. In this motivating example, $f_l(x) = h_l(x) + \delta_l(x)$ where $h_l(x)$ can denote either a weak or strong coupling expansion of order N_l , where $l = 1, \dots, K$. Meanwhile, $\delta_l(x)$ is the associated truncation error and is modeled by a GP as described in the supplementary material.

3.3 A Two-Step Approach for EFTs

Similar to Bayesian mean stacking, a two-step approach is adopted for combining the predictions across K EFTs. When constructing a two-step stacking approach, it is important to understand the available sources of information and where each can be leveraged throughout the estimation process. The first source of information is the observational data, Y_1, \dots, Y_n which are assumed to be independent random variables generated at fixed inputs $\mathbf{x}_1, \dots, \mathbf{x}_n$ according to

$$Y_i = f_{\dagger}(\mathbf{x}_i) + \epsilon_i, \quad \epsilon_i \stackrel{iid}{\sim} N(0, \sigma^2)$$

where $f_{\dagger}(\mathbf{x}_i)$ represents the true and unknown physical system. The information from the field data is collected in the set $\mathcal{D} = \{(\mathbf{x}_1, Y_1), \dots, (\mathbf{x}_n, Y_n)\}$.

Meanwhile, each EFT is also associated with its own set of information. For example, consider the l th EFT denoted by $f_l(\mathbf{x})$. It is assumed this EFT is accompanied by a set of simulator runs across a fixed set of inputs $\mathbf{x}_{l1}^c, \dots, \mathbf{x}_{ln_l}^c$. Information regarding the design of the computer experiment for each EFT can be found in Melendez et al. (2021). The simulator runs are evaluations of the finite-order expansion, $h_l(\cdot)$, at the specified inputs. Using these model runs, one can extract the set of $N_l + 1$ coefficients $c_0(\cdot), \dots, c_{N_l}(\cdot)$ at each of the fixed inputs. The training set for the l th EFT is then defined by

$$\mathcal{D}_l = \{(\mathbf{x}_{l1}^c, \mathbf{C}(\mathbf{x}_{l1}^c)), \dots, (\mathbf{x}_{ln_l}^c, \mathbf{C}(\mathbf{x}_{ln_l}^c))\}$$

where $\mathbf{C}(\cdot)$ denotes the vector of known finite-order coefficients at the specified model input. The

resulting coefficients and the set of inputs can differ across the K models, thus the sets $\mathcal{D}_1, \dots, \mathcal{D}_K$ will contain different information.

The proposed two-step approach is tailored to EFTs by taking advantage of the sources of data described above as well as the properties described in the supplementary material. The proposed Bayesian mean stacking approach extends the traditional methodologies by incorporating input-dependent weights. Conditional on the values of the theoretical predictions at a given point, $f_1(\mathbf{x}_i), \dots, f_K(\mathbf{x}_i)$, this model can be defined by

$$Y_i \mid \mathbf{f}(\mathbf{x}_i), \mathbf{w}(\mathbf{x}_i), \sigma^2 \stackrel{ind}{\sim} N(\mathbf{f}^\top(\mathbf{x}_i)\mathbf{w}(\mathbf{x}_i), \sigma^2) \quad (6)$$

where $\mathbf{f}(\mathbf{x}_i) = (f_1(\mathbf{x}_i), \dots, f_K(\mathbf{x}_i))^\top$ and $\mathbf{w}(\mathbf{x}_i) = (w_1(\mathbf{x}_i), \dots, w_K(\mathbf{x}_i))^\top$. In practice, these values are unknown and must be estimated. This problem serves as the first step of the stacking procedure.

This first step fits each model, $f_l(\mathbf{x})$, independently given data, \mathcal{D}_l . As described in the supplementary material, an EFT is fit using the finite-order coefficients to learn the unknown parameters which characterize the GP assigned to the truncation error. All of this information can be extracted from \mathcal{D}_l which implies the set of field observations is not required to fit each model. Consequently, the desired theoretical predictions can be estimated without using any of the information in \mathcal{D} . This differs from existing statistical approaches as summarized in Section 2.

Prior to learning the weights, point predictions from each EFT are required at $\mathbf{x}_1, \dots, \mathbf{x}_n$. The predictions for an EFT are computed through the posterior predictive mean which is given by

$$\hat{\mathbf{f}}_l(\mathbf{x}_i) = \hat{\mathbb{E}}^{\pi|\mathcal{D}_l} [f_l(\mathbf{x}_i)], \quad i = 1, \dots, n.$$

Additionally, the posterior variance of the predictions can be extracted if desired. This posterior predictive distribution is a Gaussian process which can be characterized by the corresponding mean and covariance functions as described in Melendez et al. (2019) (see also the supplementary material).

The objective of the second stage of the stacking procedure is to estimate the weight functions shown in (6), which is the focus of this work. Conditional on the mean predictions from the first step, the model for the observational data becomes

$$Y_i \mid \hat{\mathbf{f}}(\mathbf{x}_i), \mathbf{w}(\mathbf{x}_i), \sigma^2 \stackrel{ind}{\sim} N(\hat{\mathbf{f}}^\top(\mathbf{x}_i)\mathbf{w}(\mathbf{x}_i), \sigma^2)$$

where $\hat{\mathbf{f}}(\mathbf{x}_i) = (\hat{f}_1(\mathbf{x}_i), \dots, \hat{f}_K(\mathbf{x}_i))^\top$. The weight functions are then learned using the information contained in the field data \mathcal{D} . The next section outlines the proposed model mixing scheme which defines the weight functions using Bayesian Additive Regression Trees (BART).

4 Bayesian Additive Model Mixing Trees

4.1 Bayesian Tree Models

Bayesian tree models have become increasingly popular for modeling complex and high dimensional systems (Chipman et al., 1998). Bayesian additive regression trees are used to model an unknown mean function, $E[Y | \mathbf{x}]$ (Chipman et al., 2010). This additive approach involves summing together the predictions made from m trees and is facilitated through a Bayesian backfitting algorithm (Hastie and Tibshirani, 2000). Each tree T_j is characterized by its structure, comprised of internal and terminal nodes, along with its associated set of terminal node parameters, M_j . The internal nodes define binary partitions of the input space according to a specified splitting rule. The prior probability a node is internal is $p(\eta \text{ is internal}) = \alpha(1 + d_\eta)^{-\beta}$ where d_η is the depth of the node η , while α and β are tuning parameters. By construction, this prior penalizes tree complexity and thus ensures each tree maintains a shallow and simple structure. Given d different predictors, x_1, \dots, x_d , splitting rules are of the form $x_v < c$ for $v \in \{1, \dots, d\}$ and cutpoint c from a discretized subset of \mathbb{R} . In the simplest approach, the predictor and cutpoint associated with each splitting rule are randomly selected from discrete uniform distributions. The probabilities associated with the designation of each node along with the splitting rules for internal nodes are used to define the stochastic tree-generating prior for each tree.

The m trees are learned through MCMC, where a slight modification to each structure is proposed at every iteration of the simulation. Generally, such modifications to the tree include birth, death, perturb, or rotate as described by Chipman et al. (1998) and Pratola (2016). Proposals are then accepted or rejected using a Metropolis-Hastings step. To avoid a complex reversible jump MCMC, the algorithm depends on the integrated likelihood, which is obtained by integrating over the terminal node parameters associated with the given tree. A closed form expression for this density can be obtained with conditional conjugate priors for the terminal node parameters.

Given the tree structure, prior distributions can be assigned to each terminal node parameter. In the BART model, the priors ensure each tree explains a small yet different source of variation in the data. For continuous data, BART assigns Gaussian priors to the terminal node parameters. Assuming the data is mean centered, the prior assigned to terminal node parameter μ_{pj} in node η_{pj} is given by $\mu_{pj} | T_j \sim N(0, \tau^2)$ where $\tau = (y_{max} - y_{min}) / (2k\sqrt{m})$ with tuning parameter k . Additionally, a conjugate scaled-inverse- χ^2 prior is assigned to the variance parameter.

The traditional Bayesian regression tree model can be extended to allow for a more complex

structure in the terminal nodes. Existing extensions include linear regression (Chipman et al., 2002; Prado et al., 2021) and Gaussian processes (Gramacy and Lee, 2008). For the setting of model mixing, this work extends BART to a multivariate Gaussian terminal node model.

4.2 Model Mixing with BART

The weight functions $\mathbf{w}(\mathbf{x}) = (w_1(\mathbf{x}), \dots, w_K(\mathbf{x}))^\top$ are modeled using a sum-of-trees

$$\mathbf{w}(\mathbf{x}_i) = \sum_{j=1}^m \mathbf{g}(\mathbf{x}_i, T_j, M_j), \quad (7)$$

where $\mathbf{g}(\mathbf{x}_i, T_j, M_j)$ is the K -dimensional output of the j^{th} tree using the set of terminal node parameters, M_j , at the input, \mathbf{x}_i . This approach defines the weight functions using tree bases which are learned from the data. The amount of flexibility in the weight functions can be controlled by changing the number of trees or tuning the hyperparameters in the prior distributions.

In this application of BART, each terminal node parameter is a K -dimensional vector which is assigned a multivariate Gaussian prior. The parameter is regularized so that each tree accounts for a small amount of variation in the weight functions. For the proceeding statements, let η_{pj} represent the p th terminal on the j th tree and define its corresponding parameter by $\boldsymbol{\mu}_{pj} = (\mu_{pj1}, \dots, \mu_{pjK})^\top$. Now assume the observations $(\mathbf{x}_1, y_1), \dots, (\mathbf{x}_{n_p}, y_{n_p})$ lie in the hyper-rectangle defined by η_{pj} , where n_p is the number of observations assigned to this subregion. The model at each terminal node amounts to fitting a localized Bayesian linear regression with parameter vector $\boldsymbol{\mu}_{pj}$. Due to conditional independence, the likelihood in this node is defined by

$$L(r_1, \dots, r_{n_p} \mid T_j, \boldsymbol{\mu}_{pj}, \sigma^2) = (2\pi\sigma^2)^{-n_p/2} \exp\left(-\frac{1}{2\sigma^2} \sum_{i=1}^{n_p} \left(r_i - \hat{\mathbf{f}}^\top(\mathbf{x}_i)\boldsymbol{\mu}_{pj}\right)^2\right)$$

where $\hat{\mathbf{f}}(\mathbf{x}_i) = (\hat{f}_1(\mathbf{x}_i), \dots, \hat{f}_K(\mathbf{x}_i))^\top$ is a vector of mean predictions from each EFT and r_i is the i th residual given by $r_i = y_i - \sum_{q \neq j} \hat{\mathbf{f}}^\top(\mathbf{x}_i)g(\mathbf{x}_i, T_q, M_q)$.

Conditional on the tree structure, T_j , the terminal node parameter, $\boldsymbol{\mu}_{pj}$ is assigned a conjugate multivariate Gaussian prior, namely

$$\boldsymbol{\mu}_{pj} \mid T_j \stackrel{\text{ind}}{\sim} N_K(\boldsymbol{\beta}, \tau^2 \mathbf{I}_K) \quad (8)$$

where $\boldsymbol{\beta} = (\beta_1, \dots, \beta_K)^\top$ is a K -dimensional mean vector and \mathbf{I}_K is the identity matrix. This prior is non-informative in the sense that the mean is fixed regardless of how the input space is partitioned.

In model mixing, each simulator may perform strongly in one subregion of the input space but weakly in another. This belief can be reflected in the prior distribution of $\boldsymbol{\mu}_{pj}$ by allowing the

hyperparameters to depend on the partition of input space assigned to the given terminal node. Thus, an informative prior for $\boldsymbol{\mu}_{pj}$ can be constructed as

$$\boldsymbol{\mu}_{pj} \mid T_j \stackrel{ind}{\sim} N_K(\boldsymbol{\beta}_{pj}, \tau^2 \mathbf{I}_K)$$

where $\boldsymbol{\beta}_{pj} = (\beta_{pj1}, \dots, \beta_{pjK})^\top$. This allows the prior mean to vary depending on the tree partitions and thus reflect some sense of localized model performance. Meanwhile, the assumed covariance structure implies the K vector components $\mu_{pj1}, \dots, \mu_{pjK}$ are independent a priori.

Both of the proposed priors are conjugate, which is an important choice in BART, as it allows for a closed form expression for the marginal likelihood for the vector of residuals $\mathbf{R}_{pj} = (r_1, \dots, r_{n_p})^\top$. Additionally, the conjugate priors result in closed form expressions for the full conditional distributions of the terminal node parameters and the error variance. The derivations of these distributions are found in the Appendix. In particular, the full conditional distribution for the p th terminal node in T_j is given by

$$\boldsymbol{\mu}_{pj} \mid \mathbf{R}_{pj}, T_j, \sigma^2 \stackrel{ind}{\sim} N_K \left(\left(\frac{1}{\sigma^2} \hat{\mathbf{F}}_{pj}^\top \hat{\mathbf{F}}_{pj} + \frac{1}{\tau^2} \mathbf{I}_K \right)^{-1} \left(\frac{1}{\tau^2} \boldsymbol{\beta}_{pj} + \frac{1}{\sigma^2} \hat{\mathbf{F}}_{pj}^\top \mathbf{R}_{pj} \right), \left(\frac{1}{\sigma^2} \hat{\mathbf{F}}_{pj}^\top \hat{\mathbf{F}}_{pj} + \frac{1}{\tau^2} \mathbf{I}_K \right)^{-1} \right)$$

where $\hat{\mathbf{F}}_{pj}$ is the $n_p \times K$ design matrix with the i th row vector given by the vector $\hat{\mathbf{f}}^\top(\mathbf{x}_i)$. Meanwhile, the full conditional distribution for σ^2 is a scaled-inverse- χ^2 , i.e. $\sigma^2 \sim \nu' \lambda' / \chi_{\nu'}^2$, where

$$\nu' = n + \nu \quad \text{and} \quad \lambda' = \frac{1}{n + \nu} \left(\sum_{i=1}^n \left(y_i - \hat{\mathbf{f}}^\top(\mathbf{x}_i) \mathbf{w}(\mathbf{x}_i) \right)^2 + \nu \lambda \right).$$

4.3 Calibrating Priors

First consider the prior for the terminal node parameters. The calibration of the hyperparameters differs for the non-informative and informative priors, however both approaches are designed to ensure that each model weight $w_l(\mathbf{x})$ should prefer the interval $[0, 1]$ and be centered at a value within this region. Moreover, the functions $w_1(\mathbf{x}), \dots, w_K(\mathbf{x})$ are assumed to be independent a priori at a fixed input. This enables the prior for each weight to be calibrated marginally.

4.3.1 Non-Informative Prior

Consider a non-informative prior for the terminal node parameters. In this setting, $\boldsymbol{\mu}_{pj} \mid T_j \stackrel{iid}{\sim} N_K(\boldsymbol{\beta}, \tau^2 \mathbf{I}_K)$ for the p th terminal node parameter in the j th tree. First, fix $l \in \{1, \dots, K\}$ and $i \in \{1, \dots, n\}$ to calibrate the prior for $w_l(\mathbf{x}_i)$. Since the terminal node parameters are independent and identically distributed with a diagonal covariance structure, the prior induced on $w_l(\mathbf{x}_i)$

is the same for the remaining weight and input combinations. From (7) and (8), the induced prior on the l th model weight is $w_l(\mathbf{x}_i) \sim N(m\beta_l, m\tau^2)$. Since it is believed $w_l(\mathbf{x}_i) \in [0, 1]$ with high probability, it is plausible to set $m\beta_l = 0.5$. Consequently, $\beta_l = 0.5/m$. Thus, each weight has an equal chance to reach the “extreme” values of 0 or 1 regardless of the input location. The prior standard deviation, τ , can be selected so that $w_l(\mathbf{x}_i) \in [0, 1]$ with high probability. To do this, a confidence interval for $w_l(\mathbf{x}_i)$ is constructed such that

$$0 = 0.5 - k\tau\sqrt{m} \quad \text{and} \quad 1 = 0.5 + k\tau\sqrt{m}.$$

Subtracting the first equation from the second and solving for τ yields $\tau = \frac{1}{2k\sqrt{m}}$.

This calibration approach is very similar to the one proposed by Chipman et al. (2010). The main difference is due to the context of the problem, as it is believed the weights are predominately contained in an interval $[0, 1]$ rather than the observed range of the data, $[y_{min}, y_{max}]$. Note, this approach can also be generalized to situations where the weights are assumed to prefer the interval $[a, b]$ with high probability. Such a belief would imply $\tau = (b - a)/(2k\sqrt{m})$.

4.3.2 Informative Prior

In the informative setting, the prior mean directly depends on the partitions of the input space induced by the given tree, i.e. $\boldsymbol{\mu}_{pj} \mid T_j \sim N_K(\boldsymbol{\beta}_{pj}, \tau^2 \mathbf{I}_K)$. This prior is tailored towards EFTs, where the functional variance, $v_l(\mathbf{x}_i)$, indicates the severity of the truncation error. A larger variance within a particular subregion of the domain indicates the presence of larger truncation error meaning the EFT provides a poor approximation of the true system.

In this setting, the induced prior on the l th model weight is given by $w_l(\mathbf{x}_i) \sim N(\beta_l(\mathbf{x}_i), m\tau^2)$. The function, $\beta_l(\mathbf{x}_i)$ is interpreted as the prior mean weight function and can be defined in terms of the sum-of-trees by

$$\beta_l(\mathbf{x}_i) = \sum_{j=1}^m \sum_{b=1}^{B_j} \beta_{bjl} \mathbf{1}(\mathbf{x}_i \in \eta_{bj})$$

where B_j is the number of terminal nodes in T_j and $\mathbf{1}(\mathbf{x}_i \in \eta_{bj})$ is the indicator that \mathbf{x}_i is assigned to the terminal node η_{bj} .

To calibrate the informative prior, first obtain an initial estimate of $\beta_l(\mathbf{x}_i)$ at each input $i = 1, \dots, n$. One strategy is to utilize a set of normalized precision weights (Phillips et al., 2021). Thus, for each $l \in \{1, \dots, K\}$ and $i \in \{1, \dots, n\}$, $\beta_l(\mathbf{x}_i)$ can be estimated by a ratio of precisions,

$$\beta_l(\mathbf{x}_i) = \frac{1/v_l(\mathbf{x}_i)}{1/v_1(\mathbf{x}_i) + \dots + 1/v_K(\mathbf{x}_i)}$$

where $v_l(\mathbf{x}_i)$ is the variance of the l th model at \mathbf{x}_i . This precision weighting scheme encodes prior knowledge about each model’s relative strengths and weaknesses into the model mixing framework. Since the prior of the terminal node parameter changes conditional on the tree structure, each β_{pj} is chosen separately from the other terminal node parameters. Moreover, because the terminal node parameter $\boldsymbol{\mu}_{pj}$ is assigned a diagonal covariance structure, each of the K vector components are calibrated marginally where $\mu_{pj} \mid T_j \stackrel{ind}{\sim} N(\beta_{pj}, \tau^2)$. Without loss of generality, assume $(\mathbf{x}_1, y_1), \dots, (\mathbf{x}_{n_p}, y_{n_p})$ are assigned to the hyper-rectangle associated with the terminal node η_{pj} . Given this partition and the initial guesses of $\beta_l(x_i)$, an estimate of β_{pj} can be obtained by

$$\beta_{pj} = \frac{1}{mn_p} \sum_{i=1}^{n_p} \beta_l(\mathbf{x}_i).$$

A confidence interval for each terminal node parameter can be set to have a length of $1/m$ in order to ensure each tree is a weak learner. This is done by setting $\frac{1}{m} = 2k\tau$, which implies $\tau = \frac{1}{2km}$.

4.3.3 Variance Prior

A conjugate scaled inverse chi-square distribution with hyperparameters ν and λ is assigned to the error variance σ^2 . The value of ν controls the shape of the prior distribution; increasing ν decreases the variability and results in a prior which is more concentrated around the mode. The value of λ sets the scale of the distribution, and thus specifies the region of the domain which is assigned non-negligible mass.

To calibrate the prior, first select a value of ν to reflect the desired shape of the distribution. Common values of ν range from 3 to 10. Before selecting a value for λ , one needs an initial estimate of the error variance to help set the prior around a range of plausible values of σ^2 . Given the model set and the corresponding point predictions at each of the training points $\hat{\mathbf{f}}_l(\mathbf{x}_i)$, one can use a lightly data informed prior by setting $\hat{\sigma}^2 = \max_{l=1, \dots, K} \left\{ \min_{i=1, \dots, n} \left(y_i - \hat{\mathbf{f}}_l(\mathbf{x}_i) \right)^2 \right\}$. This crude estimate has worked well in the EFT examples discussed in Section 5 due to the small error variances associated with the controlled experiments. Given this information, one strategy is to set $\hat{\sigma}^2$ to be the mean or mode of a $\lambda\nu/\chi_\nu^2$ distribution. Mean calibration sets $\frac{\nu\lambda}{\nu-2} = \hat{\sigma}^2$, which implies $\lambda = \frac{\nu-2}{\nu} \hat{\sigma}^2$. Similarly, mode calibration sets $\frac{\nu\lambda}{\nu+2} = \hat{\sigma}^2$ which implies $\lambda = \frac{\nu+2}{\nu} \hat{\sigma}^2$.

In the simulation examples presented in Section 5, the mode calibration appears to perform the best, as it typically allocates more mass around the true variance compared to the mean calibration. Since a common belief is that each model yields accurate approximations of the true system over

some subregion of the domain, one should expect the set of minimum squared differences across the K models will unveil reliable information about the true error variance.

5 EFT Examples

This section applies the proposed model mixing methodology to three real EFT examples. The first example involves mixing a concave weak coupling expansion and convex strong coupling expansion. In this setting, the true physics model lies between the expansions, hence an interpolation of the two will adequately capture the true function. The second example involves mixing two convex expansions, each of which overestimates the true system in the intermediate range of the domain. This scenario demonstrates the benefits of applying prior regularization to the weight functions rather than imposing strict conditions such as a simplex constraint. The final example demonstrates the effectiveness of the proposed method in cases where a local expert does not exist for all subregions of the domain. An area of the domain is said to be without a local expert if none of the models under consideration adequately recovers the true underlying system.

An additional goal is to demonstrate the effectiveness of model mixing with both the non-informative and informative priors. Given no prior information of the associated model discrepancies, one should elect to use the non-informative prior. If such information is available, then the informative prior can be applied.

The following examples involve data which is independently generated according to

$$Y_i = f_{\dagger}(x_i) + \epsilon_i, \quad \epsilon_i \stackrel{iid}{\sim} N(0, \sigma^2)$$

where $i = 1, \dots, 20$, $\sigma = 0.005$, and $f_{\dagger}(x)$ is defined in (1). The 20 training points are located at inputs which are evenly spaced over the interval of 0.03 to 0.50. The error standard deviation of 0.005 was selected to mimic a controlled experiment setting. Each EFT model is fit using $n_c = 4$ evaluations of the corresponding finite-order expansion.

5.1 Example 1: Mixing Two Expansions

First, consider mixing the second order weak coupling expansion, $f_s^{(2)}(x)$ with the fourth order strong coupling expansion, $f_l^{(4)}(x)$, over the domain of $[0.03, 0.5]$ as shown in Figure 1(a). The predicted mean and corresponding posterior weight functions are shown in Figures 3 and 4 respectively. Regardless of the prior type, the BART-based mixing approach exhibits accurate mean predictions

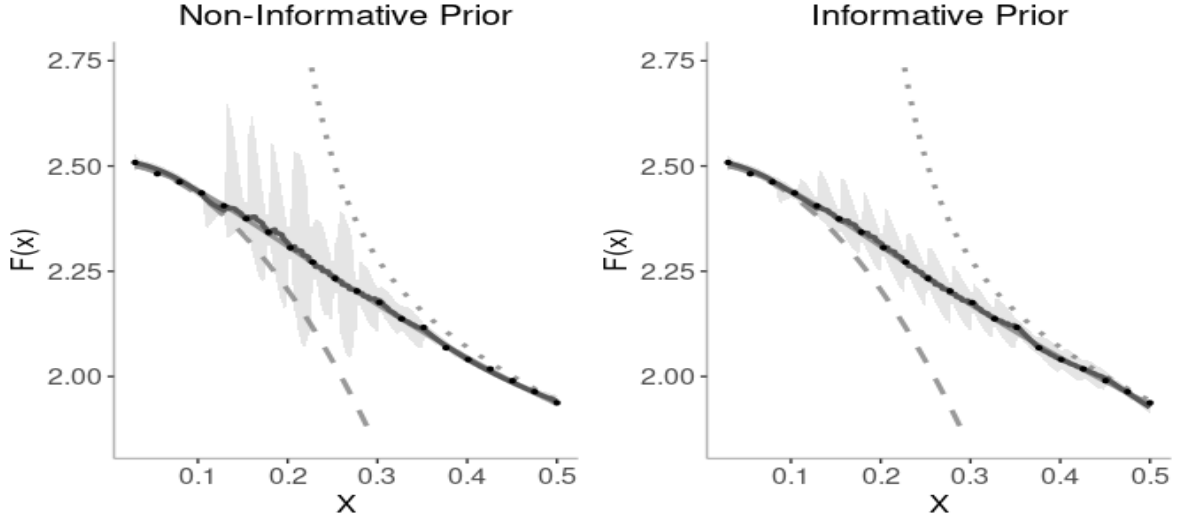


Figure 3: (Example 1) The predicted mean (dark gray) and 95% credible intervals (shaded) when mixing $f_s^{(2)}(x)$ (dashed) and $f_l^{(4)}(x)$ (dotted). The true mean (light gray) is adequately captured under both priors with a training set of 20 observations (points) and $n_c = 4$ simulator evaluations.

with minimal uncertainty in the left and right portions of the domain. The uncertainty increases in the intermediate range of the domain where neither EFT under consideration accurately predicts the true system. The most notable difference between the two approaches can be seen in the associated uncertainty within this intermediate range, as the non-informative prior typically yields wider 95% credible intervals across this region. This is plausible as the informative prior directly incorporates knowledge related to the individual model performance into its hyperparameters. Therefore, the posterior distribution of the weight functions is less dependent upon the data and is noticeably influenced by the prior. Meanwhile, the results under both priors yield similar weight functions which exhibit sigmoid-like curves. This result is intuitive of how the EFTs should be mixed, as the weak coupling expansion is appropriate in the left portion of the domain while the strong coupling is appropriate in the right region. A linear combination of these functions is useful for the intermediate range. The posterior weight functions obtained using the informative prior generally exhibit smoother shapes with less variability compared to the results under the non-informative prior. Figure 4 directly illustrates the effect of the prior on the posterior weight functions, as the informative version enables one to gain a more precise understanding of the behavior of the weight functions. This figure suggests two key insights. First, this mean mixing approach searches for useful combinations of mean predictions in order to recover the true system. Clearly, various

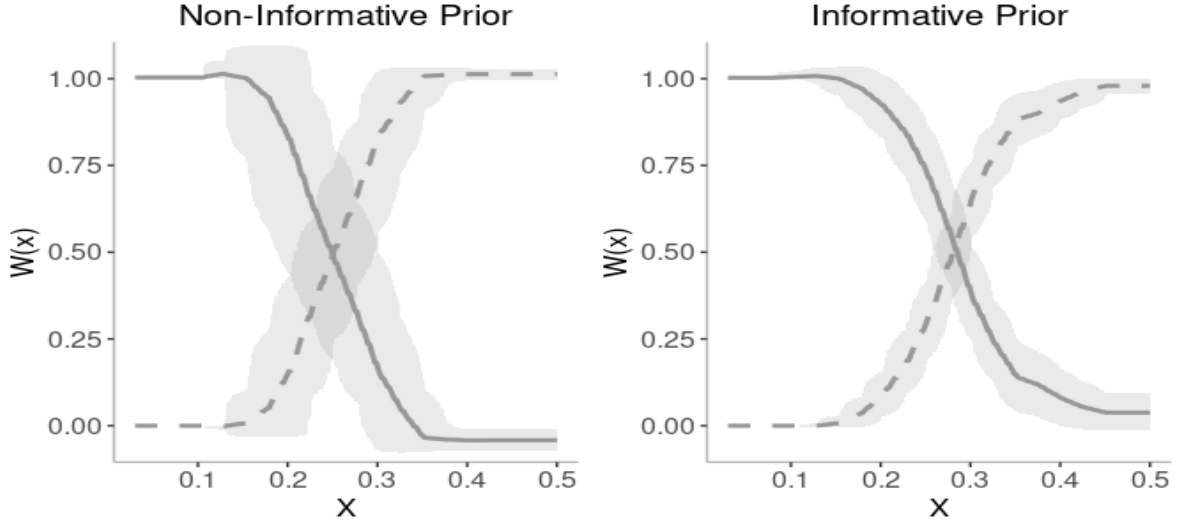


Figure 4: (Example 1) The posterior estimates of the weight functions when mixing $f_s^{(2)}(x)$ (solid) and $f_t^{(4)}(x)$ (dashed). The respective 95% credible intervals are denoted by the shaded regions.

sets of weight functions can yield very similar final predictions. Finally, the amount of variability observed in the final prediction of the physical system is directly related to the variability in the weight functions. This is evident in the results obtained with the informative prior.

5.2 Example 2: Mixing Two Convex Expansions

Now consider mixing two convex expansions which are always equal or greater than $f_{\dagger}(x)$, as shown in Figure 1(b). In this problem, a convex combination of the models in the intermediate range will never capture the true system. Meanwhile, the BART-based approach benefits from the flexibility of the prior regularization strategy as it is able to recover $f_{\dagger}(x)$.

From Figure 5, both priors lead to accurate mean predictions of the physical system. As in Example 1, the result under the informative prior yields a lower degree of uncertainty compared to its non-informative counterpart, particularly across the region of $[0.15, 0.40]$. Meanwhile, the posterior weight functions return very similar shapes under the two priors as displayed in Figure 6. Similar to Example 1, the informative prior generally results in more precise estimates of the weight functions which translates to lower uncertainty in the posterior predictions of the physical system.

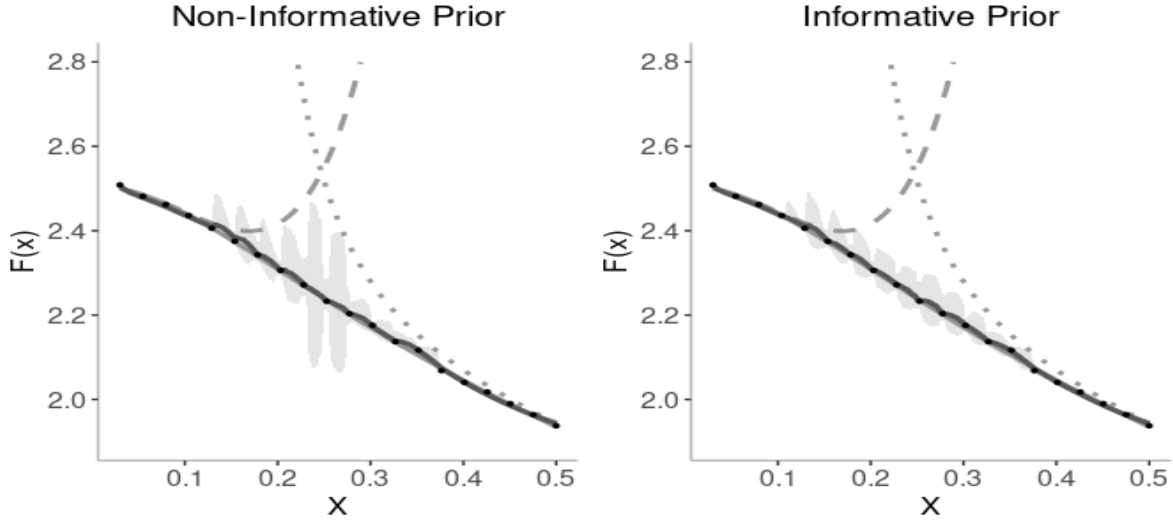


Figure 5: (Example 2) The predicted mean (dark gray) and 95% credible intervals (shaded) when mixing $f_s^{(4)}(x)$ (dashed) and $f_l^{(4)}(x)$ (dotted) to predict the true system (light grey).

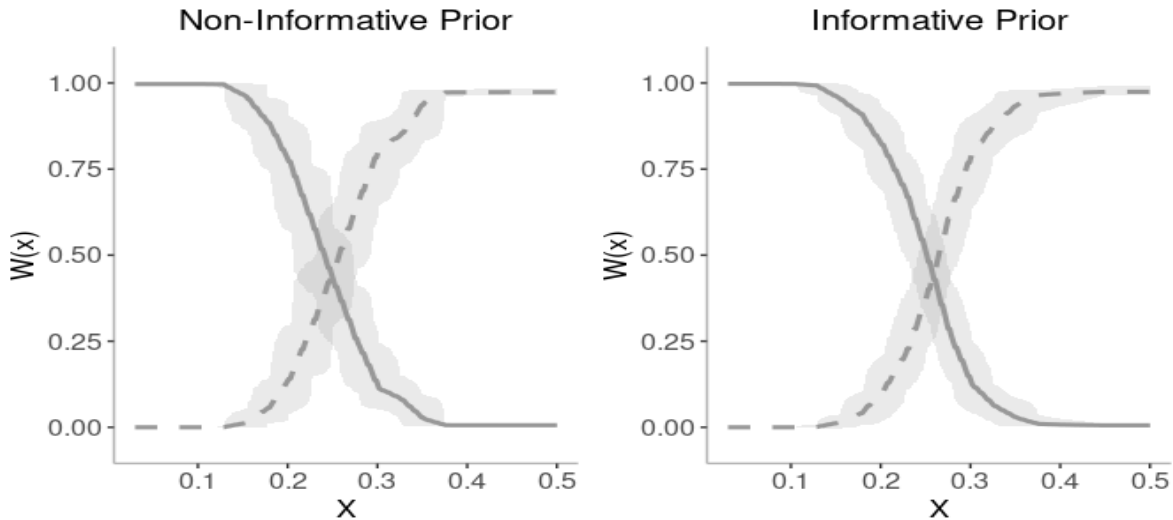


Figure 6: (Example 2) The posterior estimates of the weight functions when mixing $f_s^{(4)}(x)$ (solid) and $f_l^{(4)}(x)$ (dashed). The 95% credible intervals are denoted by the shaded regions.

5.3 Example 3: Mixing Without a Local Expert

This example demonstrates the BART-based model's ability to mix functions in regions where no local expert may exist. Consider the model set containing three weak coupling expansions of orders 2, 4 and 6 as shown in Figure 1(c). In this case, no local expert exists in the right portion of

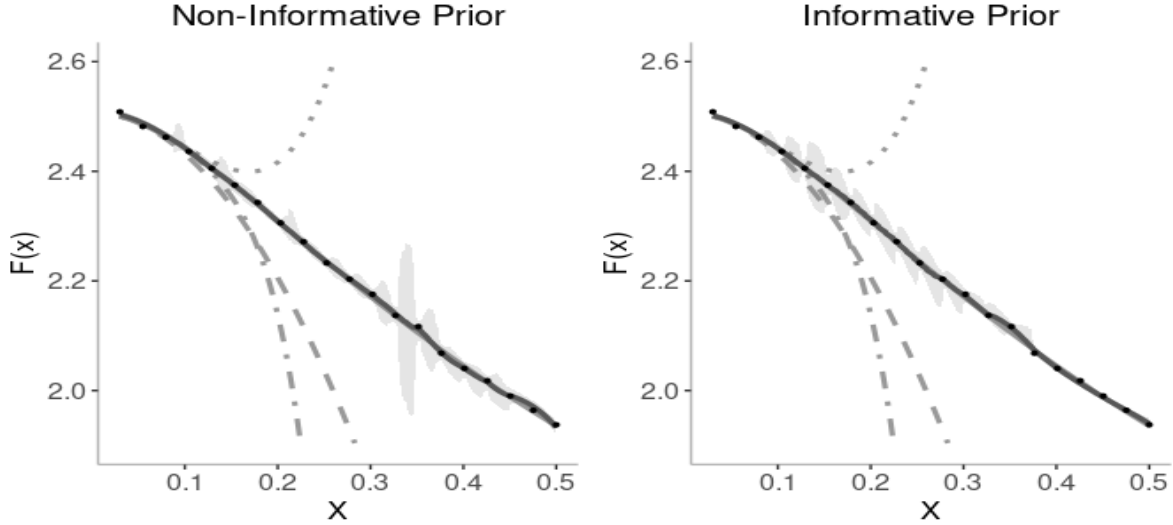


Figure 7: (Example 3) The predicted mean (dark gray) and 95% credible intervals (shaded) when mixing $f_s^{(2)}(x)$ (dashed), $f_s^{(4)}(x)$ (dotted), and $f_s^{(6)}(x)$ (dashed, dotted). The true mean (light gray) is adequately captured under both priors.

the domain as all three function diverge away from the true function at different rates.

Despite the lack of a local expert, the mixed prediction adequately recovers the true system with relatively small amounts of uncertainty as shown in Figure 7. The non-informative prior results in a greater uncertainty between $(0.3, 0.4)$, which is where the 2nd and 4th order expansions begin to diverge at quicker rates, hence the mean prediction is more sensitive to small changes in the weight values. Meanwhile, the result under the informative prior has minimal uncertainty in this right portion of the domain. Both results also display subtle deviations from $f_+(x)$ in the remainder of the domain. Overall, this example demonstrates the ability of the BART-based model to leverage observational data as well as the information in the model set to make accurate predictions.

In this example, the posterior weight functions noticeably differ depending on the selected prior, as shown in Figure 8. For example, the weight functions defined using the non-informative prior indicate more weight is allocated to the 2nd and 4th order expansions across the interval $(0.03, 0.15)$, as evident by the location of the solid and dashed curves. Additionally, all three functions have a relatively high degree of variability within this lower half of the domain. With the informative prior, a larger portion of the prediction is attributed to the 6th order expansion, which has a mean weight function around 0.6. The effects of the other two expansions are then shrunk in this lower region. As the coupling constant x increases, the 2nd order expansion contributes more to the

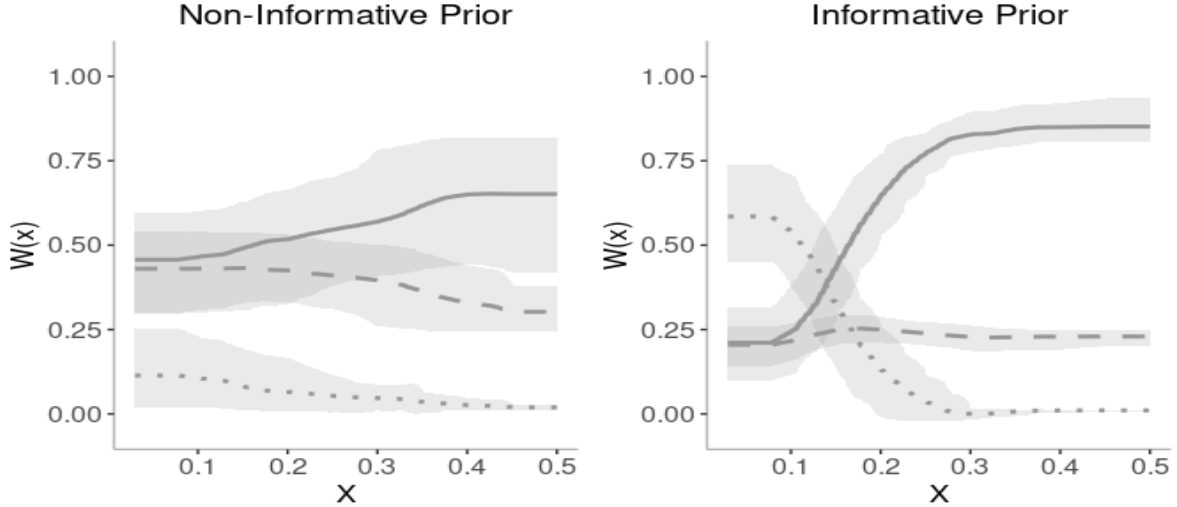


Figure 8: (Example 3) The posterior estimates of the weight functions when mixing $f_s^{(2)}(x)$ (solid), $f_s^{(4)}(x)$ (dashed), and $f_s^{(6)}(x)$ (dotted). The 95% credible intervals correspond to the shaded regions.

final prediction compared to the 4th and 6th order expansions. Finally, both approaches properly identify that the 6th order expansion diverges at a much faster rate in the right portion of the domain. Hence, its corresponding effect is shrunk to zero within this region.

This example reiterates that the BART-based approach searches for useful combinations of models, and these combinations are not unique. It also poses a more interesting question related to the interpretation of the weights. For example, in the interval $(0.03, 0.15)$, the mean predictions from each EFT are nearly identical and align closely with the true system. Given this, one may expect each EFT is assigned a weight near $1/3$, as a simple average of their predictions would be adequate in this region. However, this is not the case regardless of the prior selected. Specifically, the weight given to the 6th order expansion noticeably differs from the weights assigned to the 2nd and 4th order expansions. With the non-informative prior, this likely occurs because the trees are also regularized to be weak learners, meaning each is relatively shallow. Since the trees maintain a shallow depth, some sense of global model performance is preserved, thus the effect of the 6th order expansion is mitigated in this subregion. When considering joint credible regions, the case where all weights are near $1/3$ falls along the edge of the 99% credible region which suggests the simple average of predictions is a possibility, though it is unlikely. With the informative prior, the 6th order expansion is assigned a relatively higher weight within $(0.03, 0.15)$ because it has a smaller truncation error compared to the other models under consideration in this region.

6 Discussion

Prediction and Uncertainty Quantification

The proposed BART-based model mixing approach is able to adequately recover the underlying system $f_{\dagger}(x)$ in each of the examples presented. In general, the information from each individual model tends to dominate the posterior predictions when a local expert is present, while the information in the data is more influential in areas where no model aligns with the true system. For example, the information in the data is crucial when obtaining predictions in the intermediate range for Examples 1 and 2 or the right portion of the domain in Example 3. It should also be noted similar performance in the mean prediction is observed when the data is not evenly spaced or when the training set is reduced. In Examples 1 and 2, one should be cautious when extrapolating in the left portion of the domain due to the rapid divergence of the 4th order strong coupling expansion. However, in other settings where the rate of change for the EFT predictions is not as drastic, severe issues when extrapolating slightly outside the domain of the training data are not expected.

For each example, small levels of uncertainty in the posterior prediction of $f_{\dagger}(x)$ are observed across areas where at least one EFT aligns with the true system. The uncertainty increases in areas where the EFTs under consideration deviate from the true system. Due to the small observational errors, the mixed-model is very confident the training points align with $f_{\dagger}(x)$. As a result, the credible intervals nearly touch each training point since the predictive mean function is nearly interpolating the observations. Between training inputs, the uncertainty increases and displays a bubble-like shape. These uncertainty bands tend to smooth out when the posterior variance shifts towards high values of σ^2 as the mixed-prediction is no longer interpolating between the points.

Prior Distributions

Regardless of the prior selected, it remains clear that one is able to obtain adequate predictive performance and recover the true physical system with reasonable amounts of uncertainty. This is crucial because prior information pertaining to a model’s localized performance may not always be available. Compared to the informative prior, the results using the non-informative version will generally result in higher degrees of uncertainty across the predicted system. This is expected because there is less information about the weight functions present in the resulting posterior distributions when using the non-informative prior.

The informative prior explicitly leverages the information in the truncation errors, which directly relates to the localized predictive accuracy of each EFT. This information is used to calibrate the

prior mean of the terminal node parameters. Thus, an EFT with relatively small truncation error across a given partition of the domain will be assigned higher weight a priori compared to an EFT with relatively high errors. One can control the influence of the prior by changing the tuning parameters in the terminal node parameter model. Overall, the informative prior can be an effective tool because it essentially guides the weight functions towards the right direction using this additional model information.

Interpretation of Model Weight Functions

The primary objective of the weight functions is to re-scale the predictions given by each individual model so that a linear combination of these predictions can adequately recover the true system. Given the prior regularization method applied to the weight functions, exact interpretation of the resulting values can be unclear. However, using this regularization perspective, one can conclude that weight functions which fall close to zero within a particular input subregion indicate that the corresponding model is unnecessary for the overall prediction. Meanwhile, a model which is the unique local expert within a particular region should be weighted by values close to one. These features are observed across all three examples.

The benefit of the proposed regularization approach can further be understood through the posterior distribution of the sum of the weight functions, $w_{\text{sum}}(x) = \sum_{l=1}^K w_l(x)$. Figure 9 illustrates the posterior of $w_{\text{sum}}(x)$ for Examples 1 and 2 under the informative prior. The posterior of $w_{\text{sum}}(x)$ from Example 1 (solid) is centered very close to one with relatively small amounts of uncertainty. This results because: (i) the prior regularization and (ii) $f_+(x)$ lies between the selected EFTs, which indicates a convex combination is appropriate. Even though a sum-to-one property is not strictly imposed, it appears to naturally occur in this situation where an interpolation of the competing models is appropriate. Meanwhile, the posterior of $w_{\text{sum}}(x)$ from Example 2 (dashed) significantly drops below one in the intermediate range of the domain because both EFTs over-

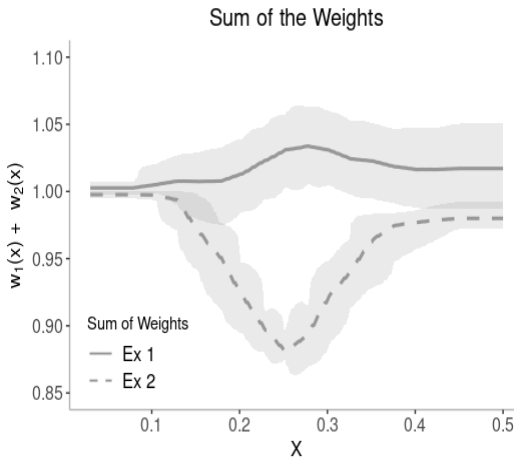


Figure 9: The posterior mean estimates and 95% credible intervals (shaded) of the sum of weight functions from Examples 1 and 2 (solid and dashed) using the informative prior.

estimate the true system, which renders a convex combination to be inappropriate. From these observations, it appears the proposed model-mixing approach benefits by not imposing strict assumptions, such as a simplex constraint, on the weights.

Additionally, one must use caution when interpreting the weight functions independently of each other. With EFTs, the weight functions are generally correlated at a fixed input. This result is intuitive in the first two examples where the predictive accuracy of the weak and strong coupling expansions are inversely related. Thus, a joint interpretation is more appropriate in these problems.

Finally, the weight functions can also be used to better understand the \mathcal{M} -open assumption associated with the model set. An initial confirmation of the \mathcal{M} -open setting can be made when the weight functions noticeably change as a function of the inputs. This observation indicates localized performance of each model, hence one can confirm the true system is not contained in the set. If the weight functions are nearly constant, one may also wish to check the posterior of $w_{\text{sum}}(x)$ to see if the sum of the weights is fixated close to one. Such a case may suggest model averaging with a simplex constraint could also be an appropriate solution. This alone is not enough to confirm or deny the \mathcal{M} -open assumption, however it may indicate that the \mathcal{M} -complete or \mathcal{M} -closed labels are possible classifications of the model set under consideration. A final case to consider is the situation where a single model receives a weight near one while the effects of the competing models are shrunk to zero across a subregion of the domain. This situation may indicate the model set is \mathcal{M} -closed conditional on the subregion of interest despite falling in the \mathcal{M} -open case when considering the entire domain at once.

In conclusion, this work proposes a Bayesian treed framework to mix predictions from a set of competing models, each of which are intended to explain the physical system across a subregion of the domain. This approach falls within the class of problems referred to as Bayesian model mixing, as input-dependent weights are defined to reflect the localized behavior of each model. The weight functions are modeled using a sum-of-trees and are regularized via a multivariate Gaussian prior. The tree bases coupled with the regularization approach allows for the weights to be learned in a flexible non-parametric manner free of strict constraints. Using the weight functions, predictions from the individual models are mixed via a linear combination. The success of this mixing approach is demonstrated on three EFT examples, each of which considers models with localized predictive performances. Leveraging the localized behavior of the individual models leads to significant improvements in the posterior prediction and uncertainty quantification of $f_+(x)$ compared to global weighting schemes.

Acknowledgements

The work of JCY and RJF work was supported in part by the National Science Foundation under Agreement OAC-2004601. The work of MTP was supported in part by the National Science Foundation under Agreements DMS-1916231, OAC-2004601, and in part by the King Abdullah University of Science and Technology (KAUST) Office of Sponsored Research (OSR) under Award No. OSR-2018-CRG7-3800.3. The work of TJS was supported in part by the National Science Foundation under Agreement DMS-1564395 (The Ohio State University).

References

- Bernardo, J. M. and Smith, A. F. (2009), *Bayesian theory*, Vol. 405, John Wiley & Sons.
- Breiman, L. (1996), “Stacked regressions”, *Machine learning* **24**(1), 49–64.
- Burgess, C. P. (2020), *Introduction to Effective Field Theory: Thinking Effectively about Hierarchies of Scale*, Cambridge University Press.
- Chipman, H. A., George, E. I. and McCulloch, R. E. (1998), “Bayesian CART model search”, *Journal of the American Statistical Association* **93**(443), 935–948.
- Chipman, H. A., George, E. I. and McCulloch, R. E. (2002), “Bayesian treed models”, *Machine Learning* **48**(1), 299–320.
- Chipman, H., George, E. and McCulloch, R. (2010), “BART: Bayesian additive regression trees”, *The Annals of Applied Statistics* **4**(1), 266–298.
- Clyde, M. and Iversen, E. S. (2013), “Bayesian model averaging in the M-open framework”, *Bayesian theory and applications* pp. 484–498.
- Draper, D. (1995), “Assessment and propagation of model uncertainty”, *Journal of the Royal Statistical Society: Series B (Methodological)* **57**(1), 45–70.
- Georgi, H. (1993), “Effective field theory”, *Ann. Rev. Nucl. Part. Sci.* **43**, 209–252.
- Gramacy, R. B. (2020), *Surrogates: Gaussian process modeling, design, and optimization for the applied sciences*, Chapman and Hall/CRC.

- Gramacy, R. B. and Lee, H. K. H. (2008), “Bayesian treed Gaussian process models with an application to computer modeling”, *Journal of the American Statistical Association* **103**(483), 1119–1130.
- Hastie, T. and Tibshirani, R. (2000), “Bayesian backfitting (with comments and a rejoinder by the authors)”, *Statistical Science* **15**(3), 196–223.
- Honda, M. (2014), “On perturbation theory improved by strong coupling expansion”, *Journal of High Energy Physics* **2014**(12), 1–44.
- Le, T. and Clarke, B. (2017), “A Bayes interpretation of stacking for M-complete and M-open settings”, *Bayesian Analysis* **12**(3), 807–829.
- Melendez, J. A., Furnstahl, R. J., Phillips, D. R., Pratola, M. T. and Wesolowski, S. (2019), “Quantifying correlated truncation errors in effective field theory”, *Physical Review C* **100**(4).
- Melendez, J., Furnstahl, R., Grießhammer, H., McGovern, J., Phillips, D. and Pratola, M. (2021), “Designing optimal experiments: an application to proton Compton scattering”, *The European Physical Journal A* **57**(3), 1–24.
- Petrov, A. A. and Blechman, A. E. (2016), *Effective Field Theories*, World Scientific.
URL: <https://www.worldscientific.com/doi/abs/10.1142/8619>
- Phillips, D., Furnstahl, R., Heinz, U., Maiti, T., Nazarewicz, W., Nunes, F., Plumlee, M., Pratola, M., Pratt, S., Viens, F. et al. (2021), “Get on the BAND wagon: a Bayesian framework for quantifying model uncertainties in nuclear dynamics”, *Journal of Physics G: Nuclear and Particle Physics* **48**(7), 072001.
- Prado, E. B., Moral, R. A. and Parnell, A. C. (2021), “Bayesian additive regression trees with model trees”, *Statistics and Computing* **31**(3), 1–13.
- Pratola, M. T. (2016), “Efficient Metropolis–Hastings proposal mechanisms for Bayesian regression tree models”, *Bayesian analysis* **11**(3), 885–911.
- Raftery, A., Madigan, D. and Hoeting, J. (1997), “Bayesian model averaging for linear regression models”, *Journal of the American Statistical Association* **92**(437), 179–191.
- Ravishanker, N., Chi, Z. and Dey, D. K. (2021), *A first course in linear model theory*, Chapman and Hall/CRC.

- Santner, T. J., Williams, B. J. and Notz, W. I. (2018), *The Design and Analysis of Computer Experiments*, 2nd ed., Springer.
- Semposki, A., Furnstahl, R. and Phillips, D. (2022), “Uncertainties here, there, and everywhere: interpolating between small-and large- g expansions using Bayesian model mixing”, *arXiv preprint arXiv:2206.04116* .
- Yang, Y. and Dunson, D. B. (2014), “Minimax optimal Bayesian aggregation”, *arXiv preprint arXiv:1403.1345* .
- Yao, Y., Pirš, G., Vehtari, A. and Gelman, A. (2021), “Bayesian hierarchical stacking: Some models are (somewhere) useful”, *Bayesian Analysis* **1**(1), 1–29.
- Yao, Y., Vehtari, A., Simpson, D. and Gelman, A. (2018), “Using stacking to average Bayesian predictive distributions”, *Bayesian Analysis* **13**(3), 917–1007.

Appendix

Let η_{pj} denote the p th terminal node in the j th tree. Without loss of generality, assume $(x_1, y_1), \dots, (x_{n_p}, y_{n_p})$ lie in the hyper-rectangle defined by η_{pj} . Furthermore, define each residual as

$$r_i = y_i - \sum_{q \neq j} \hat{\mathbf{f}}^\top(\mathbf{x}_i) \mathbf{g}(\mathbf{x}_i, T_q, M_q), \quad i = 1, \dots, n_p$$

These are collected in an n_p dimensional vector $\mathbf{R}_{pj} = (r_1, \dots, r_{n_p})^\top$. Finally, let $\hat{\mathbf{F}}_{pj}$ denote the $n_p \times K$ matrix whose l th column is $(\mathbf{f}_l(\mathbf{x}_1), \dots, \mathbf{f}_l(\mathbf{x}_{n_p}))^\top$. Due to the independence and constant variance assumptions, the model for the vector of residuals along with the associated priors is defined by

$$\begin{aligned} \mathbf{R}_{pj} \mid \boldsymbol{\mu}_{pj}, T_j, \sigma^2 &\sim N_{n_p}(\hat{\mathbf{F}}_{pj} \boldsymbol{\mu}_{pj}, \sigma^2 \mathbf{I}_{n_p}) \\ \boldsymbol{\mu}_{pj} \mid T_j &\stackrel{ind}{\sim} N_K(\boldsymbol{\beta}_{pj}, \boldsymbol{\Sigma}) \\ \sigma^2 &\sim \lambda \nu / \chi_\nu^2 \end{aligned}$$

where it is assumed $\boldsymbol{\Sigma} = \tau^2 \mathbf{I}_K$.

The Marginal Likelihood

The marginal likelihood of the residuals in node η_{pj} is defined by

$$L(\mathbf{R}_{pj} \mid T_j, \sigma^2) = \int L(\mathbf{R}_{pj} \mid T_j, \boldsymbol{\mu}_{pj}, \sigma^2) \pi(\boldsymbol{\mu}_{pj} \mid T_j) d\boldsymbol{\mu}_{pj} \quad (9)$$

Then, it follows,

$$\begin{aligned} L(\mathbf{R}_{pj} \mid T_j, \sigma^2) &= \int (2\pi\sigma^2)^{-n_p/2} \exp\left(-\frac{1}{2\sigma^2}(\mathbf{R}_{pj} - \hat{\mathbf{F}}_{pj} \boldsymbol{\mu}_{pj})^\top (\mathbf{R}_{pj} - \hat{\mathbf{F}}_{pj} \boldsymbol{\mu}_{pj})\right) \times \\ &\quad (2\pi\tau^2)^{-K/2} \exp\left(-\frac{1}{2\tau^2}(\boldsymbol{\mu}_{pj} - \boldsymbol{\beta}_{pj})^\top (\boldsymbol{\mu}_{pj} - \boldsymbol{\beta}_{pj})\right) d\boldsymbol{\mu}_{pj} \\ &= (2\pi\sigma^2)^{-n_p/2} (2\pi\tau^2)^{-K/2} \times \\ &\quad \int \left\{ \exp\left(-\frac{1}{2\sigma^2}(\mathbf{R}_{pj}^\top \mathbf{R}_{pj} - 2\boldsymbol{\mu}_{pj}^\top \hat{\mathbf{F}}_{pj}^\top \mathbf{R}_{pj} + \boldsymbol{\mu}_{pj}^\top \hat{\mathbf{F}}_{pj}^\top \hat{\mathbf{F}}_{pj} \boldsymbol{\mu}_{pj})\right) \times \right. \\ &\quad \left. \exp\left(-\frac{1}{2\tau^2}(\boldsymbol{\mu}_{pj}^\top \boldsymbol{\mu}_{pj} - 2\boldsymbol{\mu}_{pj}^\top \boldsymbol{\beta}_{pj} + \boldsymbol{\beta}_{pj}^\top \boldsymbol{\beta}_{pj})\right) d\boldsymbol{\mu}_{pj} \right\} \\ &= (2\pi\sigma^2)^{-n_p/2} (2\pi\tau^2)^{-K/2} \exp\left(-\frac{1}{2\sigma^2} \mathbf{R}_{pj}^\top \mathbf{R}_{pj} - \frac{1}{2\tau^2} \boldsymbol{\beta}_{pj}^\top \boldsymbol{\beta}_{pj}\right) \times \\ &\quad \int \exp\left(-\frac{1}{2} \boldsymbol{\mu}_{pj}^\top \left(\frac{1}{\sigma^2} \hat{\mathbf{F}}_{pj}^\top \hat{\mathbf{F}}_{pj} + \frac{1}{\tau^2} \mathbf{I}_K\right) \boldsymbol{\mu}_{pj} + \left(\frac{1}{\tau^2} \boldsymbol{\beta}_{pj} + \frac{1}{\sigma^2} \hat{\mathbf{F}}_{pj}^\top \mathbf{R}_{pj}\right)^\top \boldsymbol{\mu}_{pj}\right) d\boldsymbol{\mu}_{pj}. \end{aligned}$$

Now let $\mathbf{A}^{-1} = \frac{1}{\sigma^2} \hat{\mathbf{F}}_{pj}^\top \hat{\mathbf{F}}_{pj} + \frac{1}{\tau^2} I_K$ and $\mathbf{b} = \left(\frac{1}{\tau^2} \boldsymbol{\beta}_{pj} + \frac{1}{\sigma^2} \hat{\mathbf{F}}_{pj}^\top \mathbf{R}_{pj} \right)$. Substituting these terms into the above expression yields

$$L(\mathbf{R}_{pj} | T_j, \sigma^2) = (2\pi\sigma^2)^{-n_p/2} (2\pi\tau^2)^{-K/2} \exp\left(-\frac{1}{2\sigma^2} \mathbf{R}_{pj}^\top \mathbf{R}_{pj} - \frac{1}{2\tau^2} \boldsymbol{\beta}_{pj}^\top \boldsymbol{\beta}_{pj}\right) \times \quad (10)$$

$$\int \exp\left(-\frac{1}{2} \boldsymbol{\mu}_{pj}^\top \mathbf{A}^{-1} \boldsymbol{\mu}_{pj} + \mathbf{b}^\top \boldsymbol{\mu}_{pj}\right) d\boldsymbol{\mu}_{pj}$$

Using Lemma B.1 from Santner et al. (2018) the integral simplifies as

$$\int \exp\left(-\frac{1}{2} \boldsymbol{\mu}_{pj}^\top \mathbf{A}^{-1} \boldsymbol{\mu}_{pj} + \mathbf{b}^\top \boldsymbol{\mu}_{pj}\right) d\boldsymbol{\mu}_{pj} = (2\pi)^{K/2} |\mathbf{A}|^{1/2} \exp\left(\frac{1}{2} \mathbf{b}^\top \mathbf{A} \mathbf{b}\right). \quad (11)$$

Then, from (10) and (11), the marginal likelihood simplifies as

$$L(\mathbf{R}_{pj} | T_j, \sigma^2) = (2\pi\sigma^2)^{-n_p/2} (\tau^2)^{-K/2} |\mathbf{A}|^{1/2} \exp\left(-\frac{1}{2\sigma^2} \mathbf{R}_{pj}^\top \mathbf{R}_{pj} - \frac{1}{2\tau^2} \boldsymbol{\beta}_{pj}^\top \boldsymbol{\beta}_{pj} + \frac{1}{2} \mathbf{b}^\top \mathbf{A} \mathbf{b}\right).$$

$$= (2\pi\sigma^2)^{-n_p/2} (\tau^2)^{-K/2} \left| \left(\frac{1}{\sigma^2} \hat{\mathbf{F}}_{pj}^\top \hat{\mathbf{F}}_{pj} + \frac{1}{\tau^2} I_K \right)^{-1} \right|^{1/2}$$

$$\times \exp\left(-\frac{1}{2} \left(\frac{1}{\sigma^2} \mathbf{R}_{pj}^\top \mathbf{R}_{pj} + \frac{1}{\tau^2} \boldsymbol{\beta}_{pj}^\top \boldsymbol{\beta}_{pj} - \mathbf{b}^\top \mathbf{A} \mathbf{b} \right)\right)$$

where $\mathbf{b}^\top \mathbf{A} \mathbf{b} = \left(\frac{1}{\tau^2} \boldsymbol{\beta}_{pj} + \frac{1}{\sigma^2} \hat{\mathbf{F}}_{pj}^\top \mathbf{R}_{pj} \right)^\top \left(\frac{1}{\sigma^2} \hat{\mathbf{F}}_{pj}^\top \hat{\mathbf{F}}_{pj} + \frac{1}{\tau^2} I_K \right)^{-1} \left(\frac{1}{\tau^2} \boldsymbol{\beta}_{pj} + \frac{1}{\sigma^2} \hat{\mathbf{F}}_{pj}^\top \mathbf{R}_{pj} \right)$.

The Posterior of $\boldsymbol{\mu}_{pj}$

Now consider the full conditional posterior distribution of the terminal node parameter $\boldsymbol{\mu}_{pj}$. Using Bayes rule,

$$\pi(\boldsymbol{\mu}_{pj} | \mathbf{R}_{pj}, T_j, \sigma^2) \propto L(\mathbf{R}_{pj} | T_j, \boldsymbol{\mu}_{pj}, \sigma^2) \pi(\boldsymbol{\mu}_{pj} | T_j)$$

A conjugate prior is assumed for $\boldsymbol{\mu}_{pj}$, thus the terms in the likelihood and prior can be rearranged to obtain a Normal kernel for the posterior distribution. This process is summarized below.

$$\pi(\boldsymbol{\mu}_{pj} | \mathbf{R}_{pj}, T_j, \sigma^2) \propto \exp\left(-\frac{1}{2\sigma^2} (\mathbf{R}_{pj} - \hat{\mathbf{F}}_{pj} \boldsymbol{\mu}_{pj})^\top (\mathbf{R}_{pj} - \hat{\mathbf{F}}_{pj} \boldsymbol{\mu}_{pj})\right) \times$$

$$\exp\left(-\frac{1}{2\tau^2} (\boldsymbol{\mu}_{pj} - \boldsymbol{\beta}_{pj})^\top (\boldsymbol{\mu}_{pj} - \boldsymbol{\beta}_{pj})\right)$$

$$\propto \exp\left\{-\frac{1}{2} \left(\boldsymbol{\mu}_{pj}^\top \left(\frac{1}{\sigma^2} \hat{\mathbf{F}}_{pj}^\top \hat{\mathbf{F}}_{pj} + \frac{1}{\tau^2} I_K \right) \boldsymbol{\mu}_{pj} - 2\boldsymbol{\mu}_{pj}^\top \left(\frac{1}{\tau^2} \boldsymbol{\beta}_{pj} + \frac{1}{\sigma^2} \hat{\mathbf{F}}_{pj}^\top \mathbf{R}_{pj} \right) \right)\right\}$$

$$\propto \exp\left\{-\frac{1}{2} \left(\boldsymbol{\mu}_{pj}^\top \mathbf{A}^{-1} \boldsymbol{\mu}_{pj} - 2\boldsymbol{\mu}_{pj}^\top \mathbf{A}^{-1} \mathbf{A} \mathbf{b} \right)\right\}$$

where $\mathbf{A}^{-1} = \frac{1}{\sigma^2} \hat{\mathbf{F}}_{pj}^\top \hat{\mathbf{F}}_{pj} + \frac{1}{\tau^2} I_K$ and $\mathbf{b} = \frac{1}{\tau^2} \boldsymbol{\beta}_{pj} + \frac{1}{\sigma^2} \hat{\mathbf{F}}_{pj}^\top \mathbf{R}_{pj}$. The previous expression simplifies as

$$\pi(\boldsymbol{\mu}_{pj} | \mathbf{R}_{pj}, T_j, \sigma^2) \propto \exp\left(-\frac{1}{2} (\boldsymbol{\mu}_{pj} - \mathbf{A} \mathbf{b})^\top \mathbf{A}^{-1} (\boldsymbol{\mu}_{pj} - \mathbf{A} \mathbf{b})\right)$$

This is the kernel of a Multivariate Gaussian distribution with mean $\mathbf{A}\mathbf{b}$ and covariance matrix \mathbf{A} . Thus it follows

$$\boldsymbol{\mu}_{pj} \mid \mathbf{R}_{pj}, T_j, \sigma^2 \stackrel{ind}{\sim} N_K(\mathbf{A}\mathbf{b}, \mathbf{A})$$

replacing \mathbf{A} and \mathbf{b} with their respective definitions implies

$$\boldsymbol{\mu}_{pj} \mid \mathbf{R}_{pj}, T_j, \sigma^2 \stackrel{ind}{\sim} N_K\left(\left(\frac{1}{\sigma^2}\hat{\mathbf{F}}_{pj}^\top\hat{\mathbf{F}}_{pj} + \frac{1}{\tau^2}I_K\right)^{-1}\left(\frac{1}{\tau^2}\boldsymbol{\beta}_{pj} + \frac{1}{\sigma^2}\hat{\mathbf{F}}_{pj}^\top\mathbf{R}_{pj}\right), \left(\frac{1}{\sigma^2}\hat{\mathbf{F}}_{pj}^\top\hat{\mathbf{F}}_{pj} + \frac{1}{\tau^2}I_K\right)^{-1}\right)$$

The Posterior Distribution of σ^2

Finally, consider the full conditional posterior for the error variance, which is defined by

$$\pi(\sigma^2 \mid \mathbf{Y}, T, M) \propto L(\mathbf{Y} \mid T, M, \sigma^2)\pi(\sigma^2)$$

where $\mathbf{Y} = (y_1, \dots, y_n)^\top$, $T = \{T_1, \dots, T_m\}$, and $M = \{M_1, \dots, M_m\}$.

Further, assume a conjugate prior for σ^2 , namely $\sigma^2 \sim \nu\lambda/\chi_\nu^2$ which has a probability density function defined by

$$\pi(\sigma^2) = \frac{(\nu/2)^{\nu/2}}{\Gamma(\nu/2)}\lambda^{\nu/2}(\sigma^2)^{-(\nu/2+1)}\exp\left(-\frac{\nu\lambda}{2\sigma^2}\right)$$

Due to conjugacy, the full conditional distribution is given by

$$\begin{aligned}\pi(\sigma^2 \mid \mathbf{Y}, T, M) &\propto (\sigma^2)^{-n/2}\exp\left\{-\frac{1}{2\sigma^2}\sum_{i=1}^n\left(y_i - \hat{\mathbf{f}}^\top(\mathbf{x}_i)\mathbf{w}(\mathbf{x}_i)\right)^2\right\}(\sigma^2)^{-(\nu/2+1)}\exp\left\{-\frac{\nu\lambda}{2\sigma^2}\right\} \\ &\propto (\sigma^2)^{-(n/2+\nu/2+1)}\exp\left\{-\frac{1}{2\sigma^2}\left(\sum_{i=1}^n\left(y_i - \hat{\mathbf{f}}^\top(\mathbf{x}_i)\mathbf{w}(\mathbf{x}_i)\right)^2 + \nu\lambda\right)\right\}\end{aligned}$$

This is the kernel of another scaled inverse- χ^2 distribution, namely $\sigma^2 \sim \nu'\lambda'/\chi_{\nu'}^2$, where

$$\nu' = n + \nu \quad \text{and} \quad \lambda' = \frac{1}{n + \nu}\left(\sum_{i=1}^n\left(y_i - \hat{\mathbf{f}}^\top(\mathbf{x}_i)\mathbf{w}(\mathbf{x}_i)\right)^2 + \nu\lambda\right)$$

Supplementary Material

An Overview of EFT

EFTs model physical systems by an infinite expansion of terms organized in order of decreasing importance according to the power counting principle (Burgess, 2020; Petrov and Blechman, 2016; Georgi, 1993). Exact theoretical predictions of the system are obtained by summing over these terms. In practice, only a finite number of lower-order terms are known. Thus, the theoretical prediction can be decomposed using a Taylor-like series which includes the known finite-order expansion along with the induced truncation error. Predictions of experimental quantities can then be represented using an additive model

$$Y(x) = f_{\dagger}(x) + \epsilon(x)$$
$$f_{\dagger}(x) = h^{(N)}(x) + \delta^{(N)}(x)$$

where $x \in \mathbb{R}^d$ denotes an independent variable associated with the system, $h^{(N)}(x)$ represents the known finite-order expansion of degree N , $\delta^{(N)}(x)$ is the associated truncation error, and $\epsilon(x)$ is the random observational error. The accuracy of the finite-order expansion may vary significantly across a subspace of the domain. For example, a finite-order expansion centered about zero may yield a high fidelity approximation in the lower regions of the domain. However, the accuracy of the prediction quickly degrades in higher regions of the domain.

It is further assumed the finite-order expansion can be modeled as a stochastic process. First, the finite-order expansion can be factorized as

$$h^{(N)}(x) = y_{\text{ref}}(x) \sum_{k=0}^N c_k(x) Q^k(x), \quad (12)$$

where $y_{\text{ref}}(x)$ sets the scale of variation, $c_0(x), \dots, c_N(x)$ are dimensionless observable coefficients, and $Q(x)$ is a dimensionless expansion parameter. When the scale and expansion parameters are known based on theoretical arguments, the coefficients $c_0(x), \dots, c_N(x)$ appear to behave as a set of independent and identically distributed curves from a stochastic process. Thus, a common model for the coefficients is a Gaussian process

$$c_k(x) \mid \boldsymbol{\theta} \sim GP(\mu, \bar{c}^2 r(x, x'; \ell)) \quad (13)$$
$$\boldsymbol{\theta} = (\mu, \bar{c}^2, \ell),$$

where μ denotes a constant mean function and $\bar{c}^2 r(x, x'; \ell)$ represents the covariance function (Melendez et al., 2019). A common assumption is to set $\mu = 0$, while prior distributions can be assigned to the remaining parameters in the model (Melendez et al., 2019). Additionally, a likelihood can be formed by collecting n_c evaluations of the finite-order expansion, $\mathbf{h}^{(N)} = (h^{(N)}(x_1^c), \dots, h^{(N)}(x_{n_c}^c))^\top$, at design inputs $x_1^c, \dots, x_{n_c}^c$. These model runs are used to extract the observed finite-order coefficients, which are modeled via (13). Using the priors and the likelihood based on the model runs, the parameters in the GP are then learned through standard Bayesian inference.

The truncation error accounts for the remaining unknown terms in the series, thus $\delta^{(N)}(x)$ is modeled using a similar factorization

$$\delta^{(N)}(x) = y_{\text{ref}}(x) \sum_{k=N+1}^{\infty} c_k(x) Q^k(x). \quad (14)$$

Using (13) and (14) along with properties of the multivariate Normal distributions (Ravishanker et al., 2021), the induced prior on the truncation error term is given by

$$\delta^{(N)}(x) \mid \boldsymbol{\theta}, Q \sim GP(m_\delta(x), \bar{c}^2 R_\delta(x, x'; \ell)), \quad (15)$$

with mean and covariance functions

$$m_\delta(x) = y_{\text{ref}}(x) \frac{Q^{N+1}(x)}{1 - Q(x)} \mu \quad (16)$$

$$R_\delta(x, x'; \ell) = y_{\text{ref}}(x) y_{\text{ref}}(x') \frac{[Q(x)Q(x')]^{N+1}}{1 - Q(x)Q(x')}. \quad (17)$$

The unknown parameters in (15) - (17) originate from the coefficient model in (12). Thus, the mean and covariance functions which characterize the discrepancy model are also learned using the set of n_c evaluations of the finite-order expansion. This is a unique property of EFTs, as observational data is not required to learn the model discrepancy.

When the finite-order expansion is computationally inexpensive to evaluate, the induced prior on the theoretical predictions, $f(x) = h^{(N)}(x) + \delta^{(N)}(x)$ is given by

$$f(x) \mid \boldsymbol{\theta}, Q, \mathbf{h}^{(N)} \sim GP(m_{\text{th}}(x), \Sigma_{\text{th}}(x, x')),$$

where $m_{\text{th}}(x) = h^{(N)}(x) + m_\delta(x)$ and $\Sigma_{\text{th}}(x, x') = \bar{c}^2 R_\delta(x, x'; \ell)$. In the expensive case, a GP can be used to emulate the finite-order expansion and is defined by

$$h^{(N)}(x) \mid \boldsymbol{\theta}, Q \sim GP(m_N(x), \bar{c}^2 R_N(x, x'; \ell)).$$

The resulting prior on the theoretical prediction is a GP with mean and covariance functions $m_{\text{th}}(x) = m_N(x) + m_\delta(x)$ and $\Sigma_{\text{th}}(x, x') = \bar{c}^2 R_N(x, x'; \ell) + \bar{c}^2 R_\delta(x, x'; \ell)$. In either case, given a set of model runs $\mathbf{h}^{(N)}$, one can obtain posterior predictions $\hat{f}(\tilde{x}_1), \dots, \hat{f}(\tilde{x}_m)$ at new inputs $\tilde{x}_1, \dots, \tilde{x}_m$.